ESPRIT-Oriented Precoder Design for mmWave Channel Estimation

Musa Furkan Keskin*, Alessio Fascista†, Fan Jiang‡, Angelo Coluccia†,
Gonzalo Seco-Granados§, Henk Wymeersch*
*Chalmers University of Technology, Sweden, †University of Salento, Italy,
‡Halmstad University, Sweden, §Autonomous University of Barcelona, Spain

Abstract—We consider the problem of ESPRIT-oriented precoder design for beamspace angle-of-departure (AoD) estimation in downlink mmWave multiple-input single-output communications. Standard precoders (i.e., directional/sum beams) yield poor performance in AoD estimation, while Cramér-Rao bound-optimized precoders undermine the so-called shift invariance property (SIP) of ESPRIT. To tackle this issue, the problem of designing ESPRIT-oriented precoders is formulated to jointly optimize over the precoding matrix and the SIP-restoring matrix of ESPRIT. We develop an alternating optimization approach that updates these two matrices under unit-modulus constraints for analog beamforming architectures. Simulation results demonstrate the validity of the proposed approach while providing valuable insights on the beampatterns of the ESPRIT-oriented precoders.

Index Terms—Precoder design, beamspace ESPRIT, channel estimation, mmWave communications.

I. INTRODUCTION

Positioning in 5G relies to a large extent on the use of mmWave frequencies, with their ample bandwidth and large antenna arrays [1]–[3]. Large bandwidths offer high delay resolution but provide limited opportunities for optimization, as base stations (BSs) must use non-overlapping subcarriers for multi-BS positioning solutions. Large antenna arrays yield high angle resolution, as well as the ability to shape signals in the spatial domain, e.g., for interference control, but also for optimizing positioning performance [4]. Harnessing the improved resolution and also exploiting optimized spatial designs enhance the performance of the channel estimation routine, which detects the number of paths, and for each path estimates the geometric parameters (i.e., time-of-arrival (ToA), angle-of-arrival (AoA), angle-of-departure (AoD)) [5]. As channel estimation is a joint function among communication, positioning, and sensing, it is important to develop methods that are both accurate and of moderate complexity [6], especially for integrated sensing and communication (ISAC) systems towards 6G multi-functional wireless networks [7].

In a general pilot-based channel estimation setup, the optimal channel parameters are the maximum *a posteriori* (MAP) estimates given the received signal sequence. However, optimization methods employed in MAP estimation can involve heavy computations. On the other hand, it is notable that mmWave channels are usually sparse, due to a limited number of multipath propagation arriving at the receiver with relatively strong path gains. As a result, sparsity-inspired low-complexity channel estimation methods are developed [8]–[13]. Among them, the estimation of signal parameters via rotational invariance techniques (ESPRIT)-based channel estimation methods have been widely studied, due to their good trade-off between estimation performance and complexity [11]–[13]. Recently, ESPRIT-based approaches have been applied to the beamspace, which is attractive since analogue and/or digital beamforming structures are employed in most massive MIMO mmWave systems [13]–[15]. However, to apply beamspace ESPRIT
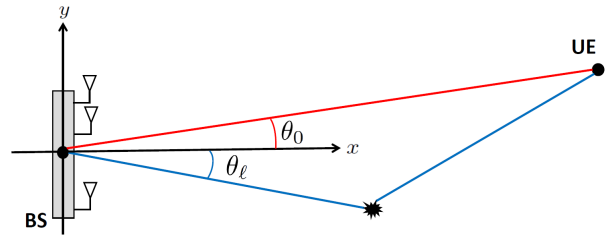
Fig. 1. mmWave MISO downlink scenario where the UE aims to estimate the AoDs of multiple paths using high-resolution beamspace ESPRIT methods.

methods, precoders are required to hold the shift invariance property (SIP). Examples of such precoding matrices include the discrete Fourier transform (DFT) beams [13], [16] and the directional beams [14]. When the SIP does not hold for the precoding matrix, an approximation will be applied during the derivation of the beamspace ESPRIT methods, leading to performance degradations [14]. In addition, research on Cramér-Rao bound (CRB)-optimized precoder design suggests that the optimal precoding matrix usually does not hold the SIP [4], [17], [18]. In other words, there is an inevitable performance loss when low-complexity ESPRIT methods are employed with CRB-optimized precoders.

In this paper, we investigate the problem of ESPRIT-oriented precoder design for AoD estimation in mmWave communications, targeting a near-optimal precoding scheme in terms of accuracy while enjoying the low-complexity and high-resolution ESPRIT methods for channel estimation. Our specific contributions are as follows:

- We formulate the problem of ESPRIT-oriented precoder design as a beampattern synthesis problem that considers joint optimization of the precoding matrix and the SIP-restoring matrix of ESPRIT.
- We propose an alternating optimization strategy that updates the precoder and the SIP-restoring matrix sequentially under the unit-modulus constraint on individual precoder elements, suitable for phase-only beamforming architectures.
- Through simulation results, we provide important insights into the beampatterns of the resulting ESPRIT-oriented precoders and demonstrate the effectiveness of the proposed design approach in ESPRIT-based channel estimation. In particular, the SIP of ESPRIT enforces uniform phase increments of complex weights across antenna elements, changing the beampattern of the CRB-optimized precoders [4], [17].

II. SYSTEM MODEL AND PROBLEM DESCRIPTION

A. System Model

We consider a mmWave MISO downlink (DL) flat-fading communications scenario with an N_{Tx}-antenna BS and a

single-antenna user equipment (UE), as shown in Fig. 1. Considering the presence of L paths[1], the received signal at the UE at transmission instance m and snapshot n is given by

$$y_{m,n} = \sqrt{P} \sum_{\ell=0}^{L-1} \alpha_{\ell,n} \mathbf{a}^{\mathsf{T}}(\theta_\ell) \mathbf{f}_m s_{m,n} + z_{m,n} \qquad (1)$$

for $m = 1,\ldots,M$ and $n = 1,\ldots,N$, where M and N denote, respectively, the number of transmissions and the number of snapshots[2]. In (1), P denotes the transmit power, $[\mathbf{a}(\theta)]_k = e^{j2\pi \frac{d}{\lambda} k \sin\theta}$, $k = 0,\ldots,N_{\mathrm{Tx}}-1$, is the steering vector for the BS TX array, $\lambda = c/f_c$ is the wavelength with c and f_c denoting the speed of propagation and carrier frequency, respectively, d is the array element spacing, $\mathbf{f}_m \in \mathbb{C}^{N_{\mathrm{Tx}} \times 1}$ denotes the BS precoder at time m, $\alpha_{\ell,n}$ and θ_ℓ are the complex channel gain and AoD of the ℓth path for the nth snapshot, respectively, $s_{m,n}$ is the pilot symbol, and $z_{m,n} \sim \mathcal{CN}(0,\sigma^2)$ is additive white Gaussian noise (AWGN) with power σ^2. For simplicity, we set $s_{m,n} = 1$, $\forall m,n$.

Aggregating the observations (1) over M transmissions, we have the received signal at the nth snapshot

$$\mathbf{y}_n = \sqrt{P} \mathbf{F}^{\mathsf{T}} \mathbf{V} \boldsymbol{\alpha}_n + \mathbf{z}_n \ , \qquad (2)$$

where $\mathbf{y}_n \triangleq [y_{1,n} \cdots y_{M,n}]^{\mathsf{T}} \in \mathbb{C}^{M \times 1}$, $\mathbf{F} \triangleq [\mathbf{f}_1 \cdots \mathbf{f}_M] \in \mathbb{C}^{N_{\mathrm{Tx}} \times M}$ is the precoding matrix satisfying $\mathrm{tr}\left(\mathbf{FF}^{\mathsf{H}}\right) = M$, $\mathbf{V} \triangleq [\mathbf{a}(\theta_0) \cdots \mathbf{a}(\theta_{L-1})] \in \mathbb{C}^{N_{\mathrm{Tx}} \times L}$, $\boldsymbol{\alpha}_n \triangleq [\alpha_{0,n} \cdots \alpha_{L-1,n}]^{\mathsf{T}} \in \mathbb{C}^{L \times 1}$, and $\mathbf{z}_n \sim \mathcal{CN}(\mathbf{0},\sigma^2\mathbf{I})$ represents the AWGN component.

B. Problem Description

In the considered mmWave scenario, the UE aims to estimate the AoDs $\boldsymbol{\theta} = [\theta_0 \cdots \theta_{L-1}]^{\mathsf{T}}$ using beamspace ESPRIT [16], [20] from the beamspace observations $\{\mathbf{y}_n\}_{n=1}^N$ in (2). The problem of interest is to design the BS precoding matrix $\mathbf{F}$ to maximize the accuracy of estimation of $\boldsymbol{\theta}$ at the UE while at the same time trying to preserve as much as possible the SIP required by ESPRIT-based estimation [16].

III. ESPRIT-ORIENTED PRECODER DESIGN

In this section, we provide a review of beamspace ESPRIT and revisit the SIP, which enforces a certain structure on the precoder. Based on this structure and using an ESPRIT-unaware baseline precoder $\mathbf{F}^{\mathrm{base}}$ (which will be introduced later in Sec. IV-A), we formulate a novel precoder design problem that jointly optimizes beampattern synthesis accuracy (with respect to $\mathbf{F}^{\mathrm{base}}$) and ESPRIT SIP error (i.e., the level of degradation of SIP), leading to near-optimal performance for ESPRIT-based estimators.

A. Review of Beamspace ESPRIT and Shift Invariance Property

From (2), we compute the sample covariance matrix

$$\widehat{\mathbf{R}} = \frac{1}{N} \sum_{n=1}^N \mathbf{y}_n \mathbf{y}_n^{\mathsf{H}} = P\mathbf{F}^{\mathsf{T}}\mathbf{V}\left(\frac{1}{N}\sum_{n=1}^N \boldsymbol{\alpha}_n \boldsymbol{\alpha}_n^{\mathsf{H}}\right)\mathbf{V}^{\mathsf{H}}\mathbf{F}^* + \sigma^2\mathbf{I} \ , \qquad (3)$$

where $\mathbf{V}$ is a Vandermonde matrix which holds the *shift invariance property* (SIP), meaning that

$$\mathbf{J}_1 \mathbf{V} = \mathbf{J}_2 \mathbf{V} \boldsymbol{\Phi}^{\mathsf{H}} \ , \qquad (4)$$

---

[1]A mmWave tracking scenario is considered with known L [17], [19].

[2]Here, snapshots may correspond to, for instance, different subcarriers of an orthogonal frequency-division multiplexing (OFDM) system. In this case, it is reasonable to assume that the channel gains $\alpha_{\ell,n}$ change across snapshots, but the AoDs θ_ℓ remain constant.

where $\mathbf{J}_1 = [\mathbf{I}_{N_{\mathrm{Tx}}-1},\ \mathbf{0}_{(N_{\mathrm{Tx}}-1)\times 1}] \in \mathbb{R}^{(N_{\mathrm{Tx}}-1)\times N_{\mathrm{Tx}}}$ and $\mathbf{J}_2 = [\mathbf{0}_{(N_{\mathrm{Tx}}-1)\times 1},\ \mathbf{I}_{N_{\mathrm{Tx}}-1}] \in \mathbb{R}^{(N_{\mathrm{Tx}}-1)\times N_{\mathrm{Tx}}}$ are selection matrices, and $\boldsymbol{\Phi} = \mathrm{Diag}([[\mathbf{a}(\theta_0)]_1, [\mathbf{a}(\theta_1)]_1, \cdots, [\mathbf{a}(\theta_{L-1})]_1]^{\mathsf{T}})$. In (3), we assume that $\frac{1}{N}\sum_{n=1}^N \boldsymbol{\alpha}_n \boldsymbol{\alpha}_n^{\mathsf{H}}$ is a diagonal matrix (i.e., paths are decorrelated), meaning that the dimension of the signal subspace is L. In the precoded case, it has been shown in [14], [16] that if the matrix $\mathbf{F}$ holds the SIP, i.e.,

$$\mathbf{J}_1 \mathbf{F} = \mathbf{J}_2 \mathbf{F} \boldsymbol{\Lambda} \qquad (5)$$

for some non-singular $\boldsymbol{\Lambda} \in \mathbb{C}^{M \times M}$, we can restore the SIP from $\mathbf{C} = \mathbf{F}^{\mathsf{T}}\mathbf{V}$, by finding a non-null matrix $\mathbf{Q}$ such that

$$\mathbf{Q}\mathbf{C}\boldsymbol{\Phi} = \mathbf{Q}\boldsymbol{\Lambda}^{\mathsf{T}}\mathbf{C} \ , \qquad (6)$$

where $\mathbf{Q} \in \mathbb{C}^{M \times M}$ satisfies

$$\mathbf{Q}[\mathbf{F}^T\mathbf{e}_M \quad \boldsymbol{\Lambda}^{\mathsf{T}}\mathbf{F}^{\mathsf{T}}\mathbf{e}_1] = \mathbf{0}, \qquad (7)$$

and $\mathbf{e}_m \in \mathbb{R}^{N_{\mathrm{Tx}} \times 1}$ is the m-th column of the identity matrix $\mathbf{I}_{N_{\mathrm{Tx}}}$. From (7), $\mathbf{Q}$ can be obtained as $\mathbf{Q} = \mathbf{I}_M - \sum_{i=0}^1 \mathbf{q}_i \mathbf{q}_i^{\mathsf{H}}$, where $\mathbf{q}_0, \mathbf{q}_1 \in \mathbb{C}^{M \times 1}$ are orthonormal column vectors spanning the subspace corresponding to $[\mathbf{F}^T\mathbf{e}_M \quad \boldsymbol{\Lambda}^{\mathsf{T}}\mathbf{F}^{\mathsf{T}}\mathbf{e}_1] \in \mathbb{C}^{M \times 2}$ [14]. Since perfect SIP cannot always be guaranteed[3] in (5), one can resort to the least-squares (LS) solution to find an approximate $\boldsymbol{\Lambda}$ [14]:

$$\widehat{\boldsymbol{\Lambda}}_{\mathrm{LS}} = \arg\min_{\boldsymbol{\Lambda}} \ \|\mathbf{J}_1\mathbf{F} - \mathbf{J}_2\mathbf{F}\boldsymbol{\Lambda}\|_F^2 \qquad (8)$$

$$= \left(\mathbf{F}^H\mathbf{J}_2^H\mathbf{J}_2\mathbf{F}\right)^{-1} \mathbf{F}^H\mathbf{J}_2^H\mathbf{J}_1\mathbf{F} \ , \qquad (9)$$

where $\|\cdot\|_F$ denotes the Frobenius norm.

Given an estimate $\widehat{\mathbf{R}}$ of the covariance matrix, the signal subspace matrix $\mathbf{U}_{\mathrm{s}} \in \mathbb{C}^{M \times L}$ can be obtained through the SVD (or truncated SVD) operation. Since both $\mathbf{C}$ and $\mathbf{U}_{\mathrm{s}}$ span the same signal subspace, we have $\mathbf{C} = \mathbf{U}_{\mathrm{s}}\mathbf{T}$, where $\mathbf{T} \in \mathbb{C}^{L \times L}$ is a non-singular matrix. Using the SIP of $\mathbf{C}$ in (6), we further obtain $\mathbf{Q}\mathbf{U}_{\mathrm{s}}\boldsymbol{\Pi} = \mathbf{Q}\boldsymbol{\Lambda}^{\mathsf{T}}\mathbf{U}_{\mathrm{s}}$ where $\boldsymbol{\Pi} = \mathbf{T}\boldsymbol{\Phi}\mathbf{T}^{-1}$. The diagonal elements in $\boldsymbol{\Phi}$ will be used to estimate the AoD of each path. The beamspace ESPRIT approach can be summarized as follows:

- Find $\boldsymbol{\Lambda}$ and $\mathbf{Q}$ for given $\mathbf{F}$.
- Obtain an estimate of the covariance matrix as $\widehat{\mathbf{R}}$ using multiple snapshots.
- Perform SVD (or truncated SVD) on $\widehat{\mathbf{R}}$ to obtain $\mathbf{U}_{\mathrm{s}}$.
- Obtain the least-square (LS) solution of $\boldsymbol{\Pi}$ as $\widetilde{\boldsymbol{\Pi}} = (\mathbf{Q}\mathbf{U}_{\mathrm{s}})^\dagger \mathbf{Q}\boldsymbol{\Lambda}^{\mathsf{T}}\mathbf{U}_{\mathrm{s}}$, where $(\cdot)^\dagger$ denotes Moore-Penrose pseudo-inverse.
- Perform eigenvalue decomposition on $\widetilde{\boldsymbol{\Pi}}$ to obtain an estimate of $\boldsymbol{\Phi}$, and retrieve the corresponding AoDs.

B. ESPRIT-Oriented Precoder Design with SIP Considerations

We formulate the problem of ESPRIT-oriented precoder design as a beampattern synthesis via joint optimization of $\mathbf{F}$ and $\boldsymbol{\Lambda}$, starting from a desired beampattern created by an ESPRIT-unconstrained precoder $\mathbf{F}^{\mathrm{base}}$ as baseline. The goal is to minimize the weighted average of the beampattern synthesis error and the ESPRIT SIP error, quantified by the error of the LS solution in (8):

$$\min_{\mathbf{F},\boldsymbol{\Lambda}} \quad \underbrace{\left\|\mathbf{B} - \mathbf{A}^{\mathsf{T}}\mathbf{F}\right\|_F^2}_{\substack{\text{beampattern synthesis} \\ \text{accuracy}}} + \eta \underbrace{\left\|\mathbf{J}_1\mathbf{F} - \mathbf{J}_2\mathbf{F}\boldsymbol{\Lambda}\right\|_F^2}_{\substack{\text{SIP approximation} \\ \text{error}}} \qquad (10a)$$

---

[3]Perfect SIP holds for DFT beams and directional/sum beams (i.e., steering vectors).

$$\text{s.t.} \quad |[\mathbf{F}]_{n,m}| = 1, \ \forall n, m \ , \tag{10b}$$

where $\mathbf{B} = \mathbf{A}^{\mathsf{T}} \mathbf{F}^{\text{base}} \in \mathbb{C}^{N_{\text{grid}} \times M}$ represents the desired beampattern corresponding to $\mathbf{F}^{\text{base}}$ at N_{grid} angular grid points $\{\theta_i\}_{i=1}^{N_{\text{grid}}}$, $\mathbf{A} = \begin{bmatrix} \mathbf{a}(\theta_1) \cdots \mathbf{a}(\theta_{N_{\text{grid}}}) \end{bmatrix} \in \mathbb{C}^{N_{\text{Tx}} \times N_{\text{grid}}}$ is the transmit steering matrix evaluated at the specified grid locations, and η is a predefined weight on the SIP error, chosen to provide a suitable trade-off between beampattern synthesis accuracy and SIP approximation error. In addition, the constraint (10b) is imposed to ensure compatibility with *phase-only beamforming* architectures [21] (e.g., analog passive arrays [22]). In the case of phase-amplitude beamforming (e.g., via active phased arrays [22]), the problem becomes the special case of (10) without the constraint (10b).

C. Alternating Optimization to Solve (10)

The problem (10) is non-convex due to *(i)* the non-convexity of (10a) in the joint variable $\mathbf{F}$ and $\mathbf{\Lambda}$, and *(ii)* the unit-modulus constraint in (10b). To tackle (10), we resort to an alternating optimization method that updates $\mathbf{F}$ and $\mathbf{\Lambda}$ in an iterative fashion.

1) Optimize $\mathbf{F}$ for fixed $\mathbf{\Lambda}$: Using the vectorization property of the Kronecker product, the objective function (10a) can be rewritten as

$$g(\mathbf{f}) \tag{11}$$
$$= \left\| \mathbf{b} - \left(\mathbf{I}_M \otimes \mathbf{A}^T \right) \mathbf{f} \right\|_2^2 + \eta \left\| \left(\mathbf{I}_M \otimes \mathbf{J}_1 - \mathbf{\Lambda}^T \otimes \mathbf{J}_2 \right) \mathbf{f} \right\|_2^2 \ ,$$

where $\mathbf{f} \triangleq \text{vec}\,(\mathbf{F})$ and $\mathbf{b} \triangleq \text{vec}\,(\mathbf{B})$. Defining

$$\mathbf{Q} \triangleq \left(\mathbf{I}_M \otimes \mathbf{A}^T \right)^H \left(\mathbf{I}_M \otimes \mathbf{A}^T \right) \tag{12}$$
$$+ \eta \left(\mathbf{I}_M \otimes \mathbf{J}_1 - \mathbf{\Lambda}^T \otimes \mathbf{J}_2 \right)^H \left(\mathbf{I}_M \otimes \mathbf{J}_1 - \mathbf{\Lambda}^T \otimes \mathbf{J}_2 \right) \ ,$$
$$\mathbf{p} \triangleq \left(\mathbf{I}_M \otimes \mathbf{A}^T \right)^H \mathbf{b} \ ,$$

the problem (10) for fixed $\mathbf{\Lambda}$ can be expressed as

$$\min_{\mathbf{f}} \ \mathbf{f}^H \mathbf{Q} \mathbf{f} - 2\Re \left\{ \mathbf{p}^H \mathbf{f} \right\} \tag{13}$$
$$\text{s.t.} \quad |f_n| = 1, \ \forall n \ .$$

The problem (13) can be solved using gradient projections iterations in [21, Alg. 1].

2) Optimize $\mathbf{\Lambda}$ for fixed $\mathbf{F}$: The subproblem of (10) for fixed $\mathbf{F}$ is exactly the LS problem defined in (8), whose solution is provided in (9).

The overall algorithm to solve (10) via alternating optimization of $\mathbf{F}$ and $\mathbf{\Lambda}$ is summarized in Algorithm 1. Based on [23, Prop. 1], Algorithm 1 converges to a stationary point of (10) if the solution to (13) is unique.

IV. SIMULATION RESULTS

To evaluate the performance of the proposed ESPRIT-oriented precoder design approach in Algorithm 1, we perform numerical simulations using a mmWave setup with $f_c = 28\,\text{GHz}$, $N_{\text{Tx}} = 64$ and $d = \lambda/2$. The signal-to-noise ratio (SNR) of the ℓth path is defined as $\text{SNR}_\ell = P|\alpha_\ell|^2/\sigma^2$. In the following parts, we first present our approach for creating baseline precoders and provide illustrative examples on beampatterns associated to ESPRIT-oriented precoders to gain insights into how ESPRIT SIP considerations change the shape of the beampatterns. Then, we evaluate the AoD estimation performance of the designed precoders.

Algorithm 1 ESPRIT-Oriented Precoder Design via Joint Optimization of $\mathbf{F}$ and $\mathbf{\Lambda}$ in (10)

1: **Input:** Baseline precoder $\mathbf{F}^{\text{base}}$, transmit steering matrix $\mathbf{A}$, selection matrices $\mathbf{J}_1$ and $\mathbf{J}_2$, SIP error weight η, convergence threshold ϵ.
2: **Output:** ESPRIT-oriented precoder $\mathbf{F}$, SIP-restoring matrix $\mathbf{\Lambda}$.
3: **Initialization:**
4: Initialize the precoder as $\mathbf{F} = \mathbf{F}^{\text{base}}$.
5: Initialize the SIP-restoring matrix as $\mathbf{\Lambda} = \widehat{\mathbf{\Lambda}}_{\text{LS}}$ via (9).
6: **Alternating Optimization Iterations:**
7: **repeat**
8:      Update $\mathbf{F}$ in (13) via [21, Alg. 1].
9:      Update $\mathbf{\Lambda}$ via (9).
10: **until** the objective (10a) converges.

A. Baseline Construction via Codebook-Based Approach

Following the idea in [4], we propose to construct the baseline precoder $\mathbf{F}^{\text{base}}$ via a codebook-based approach. Suppose that the BS has a coarse *a-priori* information on the AoDs $\boldsymbol{\theta}$ in the form of uncertainty intervals, e.g., obtained via tracking routines [4], [24], [25]. Let $\mathcal{U}_\ell = [\theta_{\min,\ell}, \theta_{\max,\ell}]$ denote the uncertainty interval for the AoD of the ℓth path and $\{\theta_{\ell,i}\}_{i=1}^{N_\ell}$ the uniformly spaced AoDs covering $\mathcal{U}_\ell$, where the grid size N_ℓ is dictated by the $3\,\text{dB}$ beamwidth angular spacing [26]. Accordingly, we define the codebook [4]

$$\mathbf{F}^{\text{base}} \triangleq \begin{bmatrix} \mathbf{F}^{\text{sum}} & \gamma \mathbf{F}^{\text{diff}} \end{bmatrix} \ , \tag{14}$$

where

$$\mathbf{F}^{\text{sum}} \triangleq \begin{bmatrix} \mathbf{F}_0^{\text{sum}} & \cdots & \mathbf{F}_{L-1}^{\text{sum}} \end{bmatrix} \ , \tag{15}$$
$$\mathbf{F}^{\text{diff}} \triangleq \begin{bmatrix} \mathbf{F}_0^{\text{diff}} & \cdots & \mathbf{F}_{L-1}^{\text{diff}} \end{bmatrix} \ , \tag{16}$$
$$\mathbf{F}_\ell^{\text{sum}} \triangleq [\mathbf{a}^*(\theta_{\ell,1}) \cdots \mathbf{a}^*(\theta_{\ell,N_\ell})] \ , \tag{17}$$
$$\mathbf{F}_\ell^{\text{diff}} \triangleq [\dot{\mathbf{a}}^*(\theta_{\ell,1}) \cdots \dot{\mathbf{a}}^*(\theta_{\ell,N_\ell})] \ , \tag{18}$$

for $\ell = 0, \ldots, L-1$, with $\dot{\mathbf{a}}(\theta) \triangleq \partial \mathbf{a}(\theta)/\partial\theta$. Here, $\mathbf{F}^{\text{sum}}$ and $\mathbf{F}^{\text{diff}}$ correspond to *sum* (directional) and *difference* (derivative) beams commonly employed in monopulse radar processing for accurate AoD estimation [27]. Similar to radar, a combined use of these beams is shown to be optimal for positioning, as well [4]. In (14), γ represents the predefined weighting factor of the difference beams with respect to the sum beams, which is set to $\gamma = 0.01$ in simulations, and $\mathbf{F}^{\text{sum}}$ and $\mathbf{F}^{\text{diff}}$ are normalized to have the same Frobenius norm before applying γ. In addition, the number of transmissions is set to $M = 2 \sum_{\ell=0}^{L-1} N_\ell$ to make the dimensions of $\mathbf{F}^{\text{base}}$ in (14) compatible with those of $\mathbf{F}$ in (2). To provide visualization and physical intuition, Fig. 2 shows the beampatterns of the sum and difference beams.

B. Illustrative Examples for ESPRIT-Oriented Precoders

Fig. 3 shows the beampatterns of the ESPRIT-oriented precoders for three different η values in Algorithm 1 by using the difference beam as the baseline. In Fig. 4, the corresponding SIP errors in (10a) are plotted with respect to η. For small η, the ESPRIT-oriented precoder has a beampattern very close to that of the difference beam since Algorithm 1 places more emphasis on beampattern synthesis accuracy than on SIP approximation error, as seen from (10a). As η increases, SIP gains more emphasis, meaning that the resulting beam approaches the sum beam, for which the SIP is perfectly satisfied, as discussed in Sec. III-A. This leads us to the following important observation.
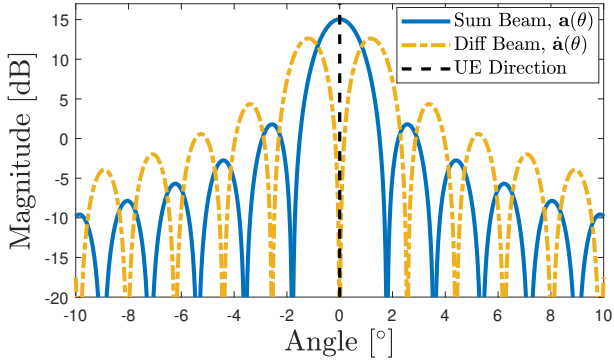
Fig. 2. Illustration of the beampatterns corresponding to the sum and difference beams in (14), steered towards the AoD $\theta = 0°$. The sum beam provides the obvious benefit of maximizing the SNR towards the desired angle, while the difference beam improves AoD accuracy in the small neighborhood around the targeted angle via its sharp curvature, which enables small angular deviations to induce large amplitude changes.

Observation 1: *Phase-only ESPRIT-oriented precoder converges from **difference beam** towards **sum beam** as η increases.*

To provide further insights, we show in Fig. 5 the phase differences across the antenna elements of the ESPRIT-oriented precoder for various η values. For small η, the ESPRIT-oriented precoder is close to the difference beam, which has a phase jump at the center of the array. The phase difference profile becomes more smooth as η increases due to the SIP requirement, which causes the resulting beam to converge to the sum beam (which has uniform phase increments). Thus, the second important observation regarding ESPRIT-oriented precoders is stated as follows.

Observation 2: *ESPRIT SIP requirement enforces **uniform phase increments** across antenna elements.*

C. Evaluation of AoD Estimation Performance

To evaluate the AoD estimation performance of the ESPRIT-oriented precoders designed via Algorithm 1, we investigate the accuracy quantified through the root mean-squared error (RMSE) of $\boldsymbol{\theta}$, i.e.,

$$\text{RMSE}_{\boldsymbol{\theta}} = \left(\mathbb{E} \left\{ \left\| \widehat{\boldsymbol{\theta}} - \boldsymbol{\theta} \right\|^2 \right\} \right)^{1/2} , \qquad (19)$$

where $\widehat{\boldsymbol{\theta}} = [\widehat{\theta}_0 \cdots \widehat{\theta}_{L-1}]^{\mathsf{T}}$ represents the estimate of $\boldsymbol{\theta}$ from $\mathbf{y}$ in (2). To obtain $\widehat{\boldsymbol{\theta}}$, we apply 1-D beamspace ESPRIT [16] described in Sec. III-A on the observations $\mathbf{y}$ in (2). We run 100 Monte Carlo trials with 50 snapshots each to construct the covariance matrix for ESPRIT at each trial. The channel gains α_ℓ are generated randomly across the snapshots by multiplying a fixed gain (determined based on SNR_ℓ) with a random zero-mean complex Gaussian coefficient with standard deviation 10. In addition, based on the results in Sec. IV-B, we set $\eta = 10^5$ in Algorithm 1. For performance benchmarking, we consider the following precoders:

- *Sum:* The precoder $\mathbf{F}^{\text{sum}}$ in (15), which by definition contains only unit-amplitude elements (i.e., steering vectors), leading to phase-only beamforming without further optimization.
- *Sum-Diff:* The precoder $\mathbf{F}^{\text{base}}$ in (14), optimized to have unit-amplitude elements by using [21, Alg. 1], which corresponds to a single $\mathbf{F}$ update step in Algorithm 1.
- *Sum-Diff, ESPRIT-Or.:* The precoder obtained via the proposed ESPRIT-oriented precoder design algorithm in Algorithm 1.

All the precoders are normalized to have the same Frobenius norm $\|\mathbf{F}\|_F$ so that the total transmit power in (2) remains the same among the different strategies for fair comparison.
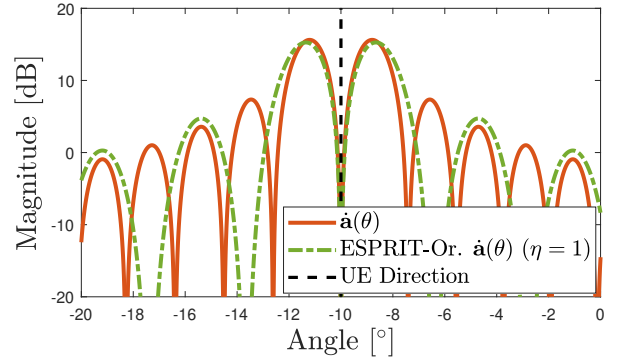
(a)
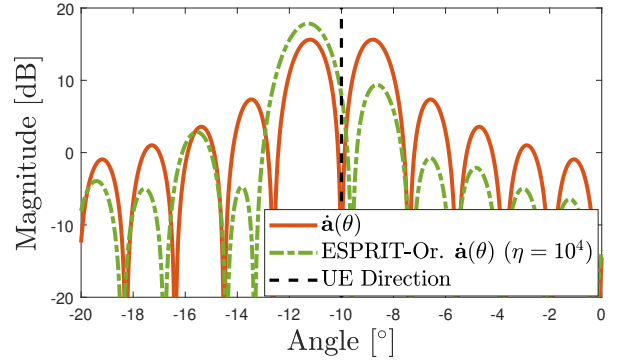
(b)
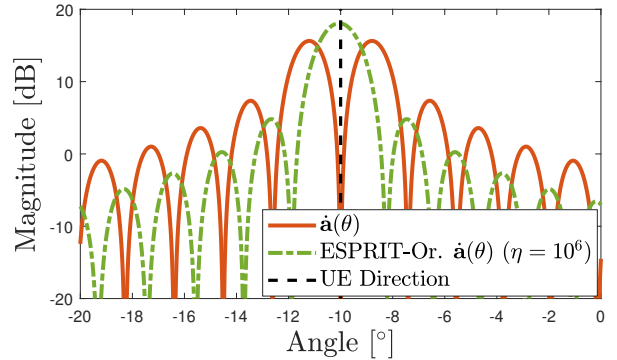
(c)

Fig. 3. The beampatterns of the ESPRIT-oriented precoders obtained via Algorithm 1 for varying η values, where the baseline precoder $\mathbf{F}^{\text{base}}$ is set to the difference beam with $\theta = -10°$.
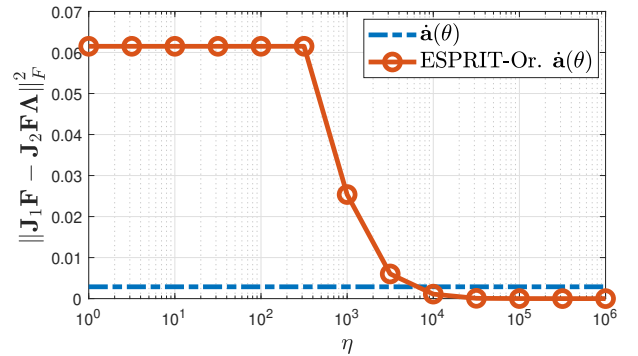
Fig. 4. SIP error in (10a) with respect to the penalty parameter η, where $\mathbf{F}^{\text{base}}$ is the difference beam with $\theta = -10°$.
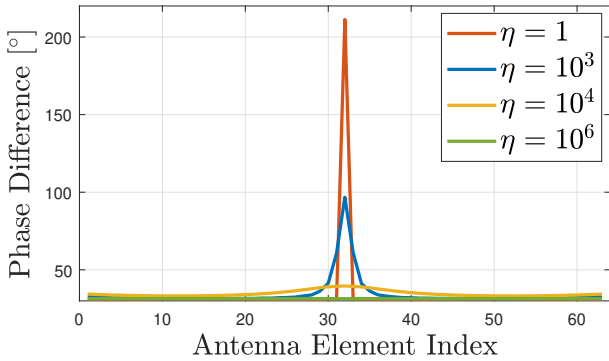
Fig. 5. Phase changes of the ESPRIT-oriented precoder obtained via Algorithm 1 across the antenna elements for varying η values, where the baseline precoder is taken as the difference beam with $\theta = -10°$.

Fig. 6. ESPRIT RMSEs obtained by the considered precoders with respect to SNR for a single-path scenario, where $\theta_0 = 20°$ and $\mathcal{U}_0 = [17°, 23°]$.

Fig. 7. ESPRIT RMSEs obtained by the considered precoders with respect to SNR for a single-path scenario, where $\theta_0 = 70°$ and $\mathcal{U}_0 = [67°, 73°]$.

We first consider a single-path scenario with $\theta_0 = 20°$ and $\mathcal{U}_0 = [17°, 23°]$. Fig. 6 shows the RMSEs obtained by the considered precoding strategies as a function of the SNR, also in comparison with the CRB[4]. It can be observed that the ESPRIT-oriented precoder provides noticeable improvement over the ESPRIT-unaware conventional sum-diff precoder at low SNRs, indicating the effectiveness of the proposed design strategy in Algorithm 1. However, the conventional sum precoder outperforms the ESPRIT-oriented design at low SNRs, while the RMSEs of all the precoders converge to the CRB as the SNR increases. This suggests that although Algorithm 1 succeeds in improving the performance, the sum precoder appears to be the best choice in this specific scenario.

Next, we consider a different setting with $\theta_0 = 70°$ and $\mathcal{U}_0 = [67°, 73°]$, whose results are reported in Fig. 7. We observe that the proposed ESPRIT-oriented design significantly outperforms both the traditional sum precoder and sum-diff precoder in the medium and high SNR regimes, closing the gap to the CRB. Comparing Fig. 6 and Fig. 7, it is seen that performance gains provided by Algorithm 1 depend on the AoD of the path. To further investigate this point, we plot in Fig. 8 the RMSE with respect to the path AoD for a fixed SNR of $20\,\mathrm{dB}$ with varying degrees of angular uncertainty. A common observation is that for all AoDs, the ESPRIT-oriented sum-diff precoder outperforms the standard sum-diff precoder, which does not consider the ESPRIT SIP conditions, suggesting that Algorithm 1 can provide considerable accuracy gains in ESPRIT-based estimation. For $\pm 1°$ uncertainty, the ESPRIT-oriented precoder achieves lower RMSE than the sum precoder for $\theta \in [-60°, 60°]$ in agreement with [4], while the trend becomes the opposite outside this interval. Looking at the $\pm 3°$ uncertainty case, the sum precoder performs slightly better than the ESPRIT-oriented one around $\theta = 0°$, while the latter can significantly outperform the former at the end-fire of the array, i.e., when the absolute value of the AoD is above $60°$. Furthermore, for the $\pm 5°$ uncertainty case, the proposed ESPRIT-oriented design provides substantial gains over the sum precoder for almost the entire range of AoD values, which further evidences the effectiveness of the proposed algorithm.

Finally, we investigate the RMSE performances for a two-path scenario with $\boldsymbol{\theta} = [20°, 70°]$, $\mathcal{U}_0 = [17°, 23°]$, $\mathcal{U}_1 = [67°, 73°]$, and $\mathrm{SNR} = [20, 0]\,\mathrm{dB}$. Fig. 9 plots the RMSE with respect to the SNR of the second path, where the SNRs of both paths are changed simultaneously while keeping their difference fixed. It is observed that the proposed ESPRIT-based design achieves higher accuracy than the benchmark schemes

---

[4]Since the CRBs belonging to the different precoders are very close to each other, we only show the CRB corresponding to $\mathbf{F}^{\mathrm{sum}}$ for the sake of figure readability.
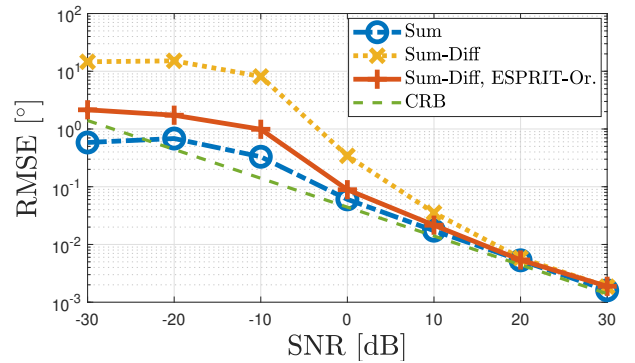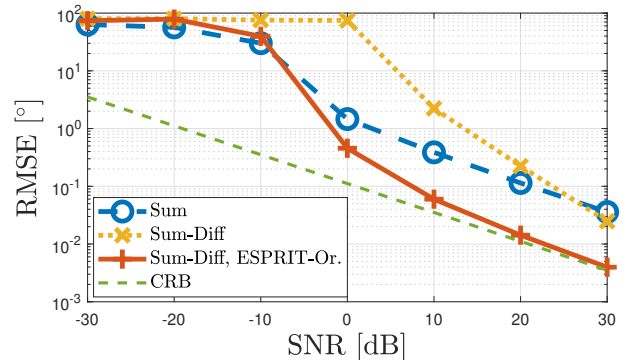
in the medium and high SNR regimes. The gap to the CRB can be attributed to the intrinsic suboptimality of ESPRIT [28], [29] and to imperfect decorrelation of the paths in the estimated correlation matrix $\widehat{\mathbf{R}}$.

V. Concluding Remarks

In this paper, we have studied the problem of mmWave precoder design tailored specifically to ESPRIT-based channel estimation. Considering the fact that standard precoders (i.e., sum beam) fail to achieve satisfactory performance in AoD estimation and that CRB-optimized precoders (sum-diff beam) destroy the SIP of ESPRIT, leading to large degradations in ESPRIT accuracy, we have developed a novel ESPRIT-oriented precoder design approach that jointly optimizes the precoder and the SIP-restoring matrix used in ESPRIT. Simulation results have provided valuable insights into how the SIP requirement impacts the beampattern of the ESPRIT-oriented precoders and shown the effectiveness of the proposed design strategy. As future work, similar design principles can be employed to extend the current study to higher dimensions, i.e., 2-D uniform rectangular arrays (URAs) at both the BS and the UE sides, possibly with OFDM transmission, leading to ESPRIT-oriented precoder and combiner designs for 5-D channel estimation (AoD, AoA and delay) [14].

References

[1] S. Bartoletti *et al.*, "Positioning and sensing for vehicular safety applications in 5G and beyond," *IEEE Communications Magazine*, vol. 59, no. 11, pp. 15–21, 2021.
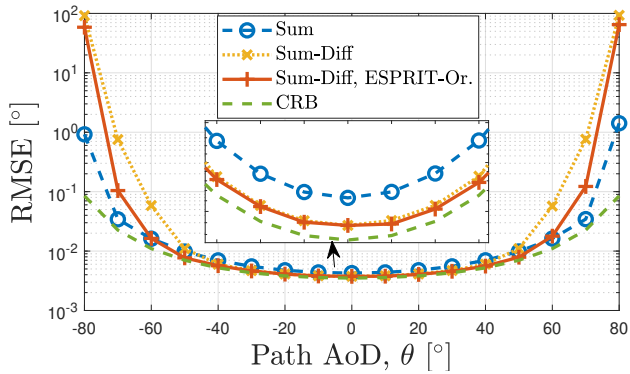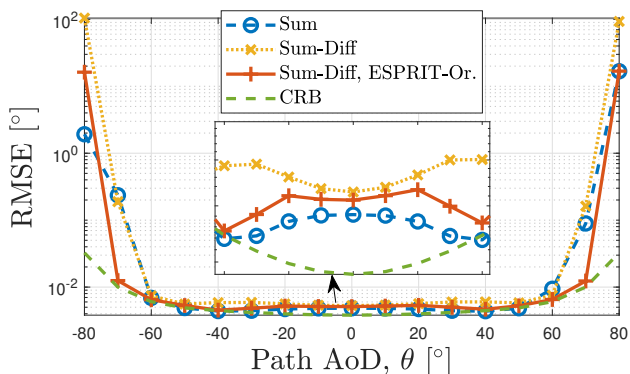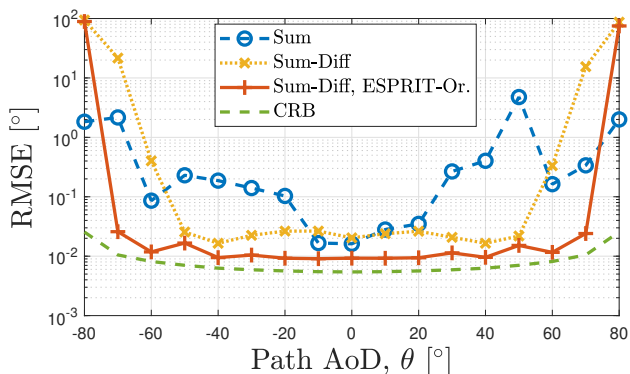
Fig. 8. ESPRIT RMSEs obtained by the considered precoders with respect to the path AoD for a single-path scenario with (a) ±1, (b) ±3, and (c) ±5 degrees of angular uncertainty for SNR = 20 dB.
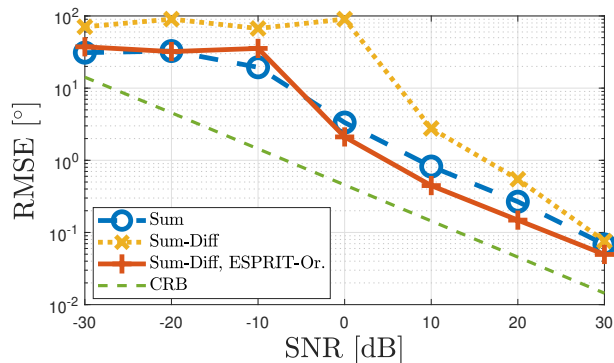
Fig. 9. ESPRIT RMSEs obtained by the considered precoders with respect to SNR for a two-path scenario, where $\boldsymbol{\theta} = [20°, 70°]$ with ±3 degrees of uncertainty for both paths.

[2] S. Dwivedi et al., "Positioning in 5G networks," IEEE Communications Magazine, vol. 59, no. 11, pp. 38–44, 2021.

[3] A. Fascista et al., "Low-complexity accurate mmwave positioning for single-antenna users based on angle-of-departure and adaptive beamforming," in IEEE International Conference on Acoustics, Speech and Signal Processing (ICASSP), 2020, pp. 4866–4870.

[4] M. F. Keskin et al., "Optimal spatial signal design for mmwave positioning under imperfect synchronization," IEEE Transactions on Vehicular Technology, vol. 71, no. 5, pp. 5558–5563, 2022.

[5] 3rd Generation Partnership Project (3GPP), "Study on NR positioning support TR 38.855," Technical Specification Group Radio Access Network, 2019.

[6] A. Fascista et al., "Low-complexity downlink channel estimation in mmwave multiple-input single-output systems," IEEE Wireless Communications Letters, vol. 11, no. 3, pp. 518–522, 2022.

[7] J. A. Zhang et al., "An overview of signal processing techniques for joint communication and radar sensing," IEEE Journal of Selected Topics in Signal Processing, vol. 15, no. 6, pp. 1295–1315, 2021.

[8] Y. Tsai et al., "Millimeter-wave beamformed full-dimensional mimo channel estimation based on atomic norm minimization," IEEE Transactions on Communications, vol. 66, no. 12, pp. 6150–6163, 2018.

[9] J. Lee et al., "Channel estimation via orthogonal matching pursuit for hybrid mimo systems in millimeter wave communications," IEEE Transactions on Communications, vol. 64, no. 6, pp. 2370–2386, 2016.

[10] A. Alkhateeb et al., "Channel estimation and hybrid precoding for millimeter wave cellular systems," IEEE journal of selected topics in signal processing, vol. 8, no. 5, pp. 831–846, 2014.

[11] F. Jiang et al., "High-dimensional channel estimation for simultaneous localization and communications," in 2021 IEEE WCNC, Nanjing, China, 2021.

[12] F. Wen et al., "5G positioning and mapping with diffuse multipath," IEEE Transactions on Wireless Communications, vol. 20, no. 2, pp. 1164–1174, 2021.

[13] J. Zhang et al., "Gridless channel estimation for hybrid mmwave MIMO systems via tensor-ESPRIT algorithms in DFT beamspace," IEEE Journal of Selected Topics in Signal Processing, vol. 15, no. 3, pp. 816–831, 2021.

[14] F. Jiang et al., "Beamspace multidimensional ESPRIT approaches for simultaneous localization and communications," 2021. [Online]. Available: https://arxiv.org/abs/2111.07450

[15] F. Wen et al., "Tensor decomposition based beamspace ESPRIT for millimeter wave mimo channel estimation," in IEEE GLOBECOM, Abu Dhabi, United Arab Emirates, 2018.

[16] G. Xu et al., "Beamspace ESPRIT," IEEE Transactions on Signal Processing, vol. 42, no. 2, pp. 349–356, 1994.

[17] N. Garcia et al., "Optimal precoders for tracking the AoD and AoA of a mmWave path," IEEE Transactions on Signal Processing, vol. 66, no. 21, pp. 5718–5729, Nov 2018.

[18] A. Fascista et al., "RIS-aided joint localization and synchronization with a single-antenna receiver: Beamforming design and low-complexity estimation," IEEE Journal of Selected Topics in Signal Processing, vol. 16, no. 5, pp. 1141–1156, 2022.

[19] D. Zhang et al., "Beam allocation for millimeter-wave MIMO tracking systems," IEEE Transactions on Vehicular Technology, vol. 69, no. 2, pp. 1595–1611, 2020.

[20] R. Roy et al., "ESPRIT-estimation of signal parameters via rotational invariance techniques," IEEE Transactions on Acoustics, Speech, and Signal Processing, vol. 37, no. 7, pp. 984–995, Jul. 1989.

[21] J. Tranter et al., "Fast unit-modulus least squares with applications in beamforming," IEEE Transactions on Signal Processing, vol. 65, no. 11, pp. 2875–2887, 2017.

[22] S. H. Talisa et al., "Benefits of digital phased array radars," Proceedings of the IEEE, vol. 104, no. 3, pp. 530–543, 2016.

[23] A. Aubry et al., "A new sequential optimization procedure and its applications to resource allocation for wireless systems," IEEE Transactions on Signal Processing, vol. 66, no. 24, pp. 6518–6533, 2018.

[24] J. C. Aviles et al., "Position-aided mm-wave beam training under NLOS conditions," IEEE Access, vol. 4, pp. 8703–8714, 2016.

[25] R. Mendrzik et al., "Enabling situational awareness in millimeter wave massive MIMO systems," IEEE Journal of Selected Topics in Signal Processing, vol. 13, no. 5, pp. 1196–1211, 2019.

[26] J. A. Zhang et al., "Multibeam for joint communication and radar sensing using steerable analog antenna arrays," IEEE Transactions on Vehicular Technology, vol. 68, no. 1, pp. 671–685, 2018.

[27] U. Nickel, "Overview of generalized monopulse estimation," IEEE Aerospace and Electronic Systems Magazine, vol. 21, no. 6, pp. 27–56, 2006.

[28] B. Ottersten et al., "Performance analysis of the total least squares ESPRIT algorithm," IEEE Transactions on Signal Processing, vol. 39, no. 5, pp. 1122–1135, 1991.

[29] F. Li et al., "Performance analysis for DOA estimation algorithms: unification, simplification, and observations," IEEE Transactions on Aerospace and Electronic Systems, vol. 29, no. 4, pp. 1170–1184, 1993.